Sliding-mode control, dynamic assessment and practical implementation of a bidirectional buck/boost DC-to-DC converter

Anthony Gee,
Student Member IEEE
DEPT OF ELECTRICAL AND ELECTRONIC ENGINEERING
University of Bath
Bath, BA2 7AY, UK
Tel.: +44 (0) 1225 386059
Fax: +44 (0) 1225 386305
ag322@bath.ac.uk

Dr. F. V. P. Robinson,
Member IEEE
DEPT OF ELECTRICAL AND ELECTRONIC ENGINEERING
University of Bath
Bath, BA2 7AY, UK
Tel.: +44 (0) 1225 383899
Fax: +44 (0) 1225 386305
F.V.P.Robinson@bath.ac.uk

Dr. R. W. Dunn,
Member IEEE
DEPT OF ELECTRICAL AND ELECTRONIC ENGINEERING
University of Bath
Bath, BA2 7AY, UK
Tel.: +44 (0) 1225 386059
Fax: +44 (0) 1225 386305
R.W.Dunn@bath.ac.uk

Acknowledgements

The authors would like to thank EPSRC Supergen Energy Storage Consortium for supporting this project.

Keywords

« Sliding mode control », « Converter control », « Energy storage », « Regenerative power », « Supercapacitor »

Abstract

Bidirectional power converters are frequently applied when interfacing energy-storage devices such as supercapacitors, uninterruptible-power-supply batteries and generators, electric-vehicle motors and renewable-energy-system generators. This paper presents a bidirectional half bridge DC/DC converter, featuring a novel sliding-mode controller, input and output short-circuit protection and a wide input voltage operating range. The ability to achieve step-up or step-down voltage conversion and accommodate a wide input voltage variation makes this design particularly useful for interfacing energy storage devices whose voltage varies widely with state of charge such as supercapacitor modules. The control theory and design methodology are described and converter performance is assessed at realistic operating levels by simulation and experiment. Benefits are shown to include good performance over a wide range of operating conditions and a relatively simple controller-hardware requirement.

Introduction

Typically, the control of DC-to-DC converters by classical linear methods has frequently been based on state-space averaging and linearisation about an operating point to obtain a small-signal transfer function which is approximately valid over a limited operating region [1]. In the case of buck/boost and boost topologies, the transfer function generally contains at least one right half plane zero [2] which complicates controller design. As the system transfer function quickly varies with circuit operating conditions, large-signal response cannot be guaranteed making the control system design even less convenient. However, since a switched-mode DC-to-DC converter constitutes a variable structure, system a sliding-mode control strategy for variable-structure systems may be employed which gives the DC-to-DC converter system greater large-signal stability and robustness to parameter variation.

In the developed power converter employing sliding-mode control, pulse width modulation (PWM) is achieved using variable-frequency current hysteresis control, which gives good dynamic performance

over a wide input voltage range of 5 V to 100 V when delivering an output of around 12 V. It also overcomes the sub-harmonic oscillation instability that occurs at duty ratios above 50% [3] in conventional power converters employing conventional fixed-frequency PWM current-mode control, which requires the further complexity of slope compensation to resolve.

Converter model and Sliding Mode controller

The developed half-bridge converter topology is illustrated in Fig. 1. The controlled variable is the output voltage V_o and V_o* represents the command reference voltage. V_b and V_g represent DC voltage sources, and R represents resistance in series with the source V_b. For example, in the case of a simplified battery-load model, R represents the internal resistance and V_b represents the internal voltage source which is dependent on state of charge. This model and the following analysis may also be applied to a uni-directional converter by setting V_b to zero.

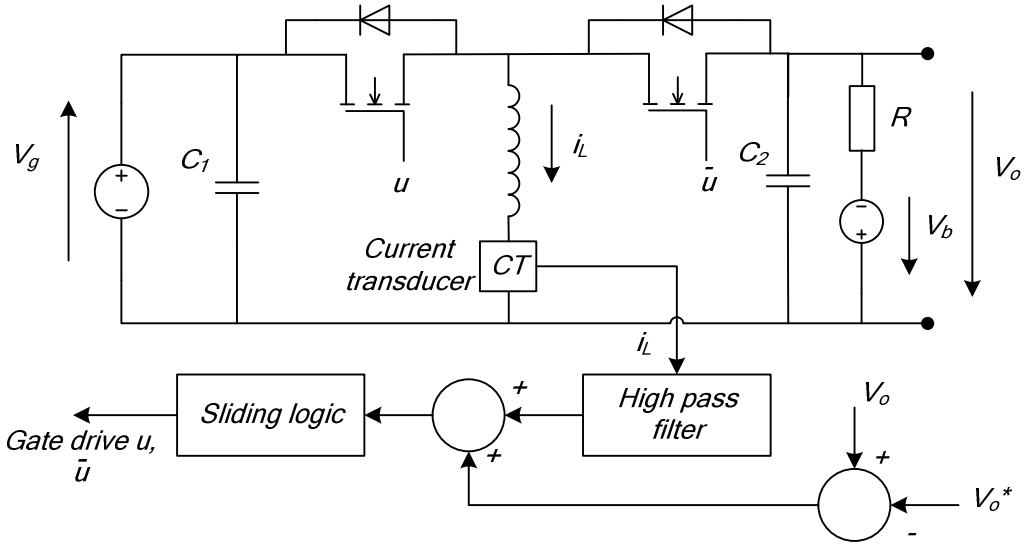

Fig. 1. Bidirectional buck / boost half bridge converter.

Defining u and $\bar{u}$ as the gate-drive logic state as shown in Fig. 1, the equations describing this system are as follows:

$$L\frac{di_L}{dt} = v_g u - v_o \bar{u} = u(v_g + v_o) - v_o \tag{1}$$

$$C\frac{dv_o}{dt} = i_L \bar{u} - \frac{v_o - v_b}{R} = i_L(1-u) - \frac{v_o - v_b}{R} \tag{2}$$

Using the same technique as in [4], the output voltage and inductor current are defined in terms of the sum of their steady-state values (shown with an *) and an error term (shown with a ^):

$$v_o = V_o^* + \hat{v}_o \; and \; i_L = I_L^* + \hat{i}_L \tag{3}$$

To control the output voltage, a sliding surface defined in terms of the controlled variable, *Vo*, and its derivative, *dVo/dt* as used in [5] is not feasible, since this derivative is discontinuous (see equation[2]). Instead, a sliding surface, σ, is defined in terms of output voltage error and current error in a similar approach to that described by Ramanarayanan [4] as follows:

$$\sigma = k_v \hat{v}_o + k_i \hat{i}_L = 0 \tag{4}$$

k_i and k_v are the gains associated with the voltage and inductor current error measurement circuits. In this prototype converter the inductor current and output voltage are measured by LEM Hall-effect transducers providing galvanic isolation between high current and voltage connections and the controller.

Conditions for Existence of a Sliding Mode and for Reaching the Sliding Surface

To ensure the existence of a sliding mode, a switching control law must be chosen which ensures that the position of the system trajectory relative to the sliding surface and its time derivative have opposite signs [6]:

$$\sigma\dot{\sigma} < 0 \forall \sigma \neq 0 \tag{5}$$

To ensure that the system reaches the sliding surface $\sigma = 0$ in finite time, condition (5) must be true and $|\dot{\sigma}|$ must be bounded by a non zero lower bound, μ [6]:

$$\sigma\dot{\sigma} < 0 \forall \sigma \neq 0 \qquad \textit{and} \qquad |\dot{\sigma}| \geq \mu > 0 \tag{6}$$

The switching control law is chosen as follows:

$$u = \begin{cases} 1, & if \quad \sigma < 0 \\ 0, & if \quad \sigma > 0 \end{cases} \tag{7}$$

Substituting u = 1 into (1) and (2), then using equation (4):

$$[\dot{\sigma}]_{u=1} = k_i \frac{v_g}{L} - k_v \frac{(v_o - v_b)}{R \cdot C} \tag{8}$$

and when u = 0:

$$[\dot{\sigma}]_{u=0} = k_v \left[\frac{i_L}{C} - \frac{(v_o - v_b)}{R \cdot C} \right] - k_i \frac{v_0}{L} \tag{9}$$

The conditions for the existence of a sliding mode (5) and equations (8) and (9) give the following inequalities for choice of inductor value to ensure existence of a sliding mode:

$$L < \frac{k_i v_g R \cdot C}{k_v (v_o - v_b)} \tag{10}$$

$$L < \frac{k_i v_o C}{k_v \left[i_L - \frac{(v_o - v_b)}{R} \right]} \tag{11}$$

In applications where V_b and V_g can vary, L, C, k_i and k_v are chosen such that the existence of a sliding mode is ensured over the operating range. The reachability condition (6) can also be ensured if the inductance is chosen in this way.

A graphical representation of the switching control action is shown in Fig. 2.

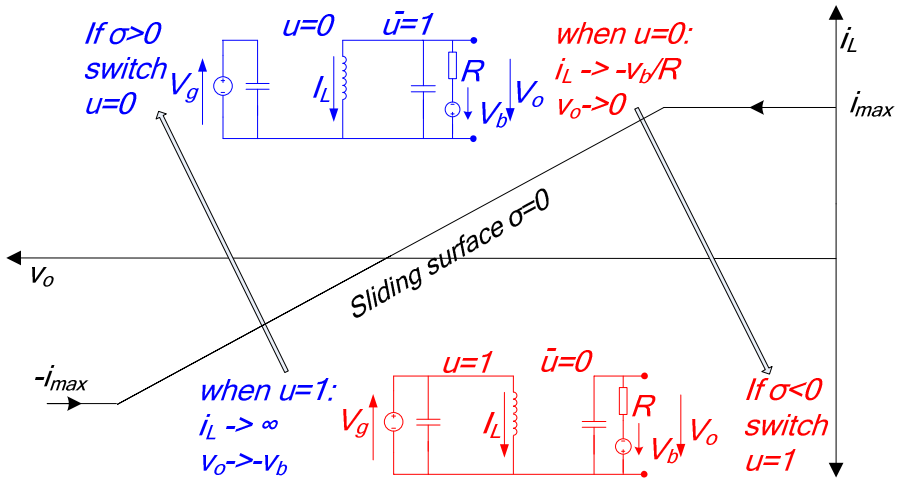

Fig. 2. Graphical representation of switching control law.

The inductor current tends to V_g / R_L as opposed to infinity for switch state u =1 but the reaching conditions are still fulfilled if inductor resistance, R_L, is kept very small in comparison to V_g.

This implementation of the sliding surface incorporates a modification to limit inductor current. The modified sliding line is made up of three straight lines and can be expressed as follows:

$$\begin{aligned} \sigma^* &= k_v \hat{v}_o + k_i \hat{i}_L = 0 \quad If -i_{\max} \le i_l \le i_{\max} \\ \sigma^* &= i_{\max} - i_L = 0 \quad If \ i_l > i_{\max} \\ \sigma^* &= -i_{\max} - i_L = 0 \quad If \ i_l < -i_{\max} \end{aligned} \tag{12}$$

This is done to limit an otherwise high transient current at start-up when the voltage error can be high, particularly if the voltage gain k_v is much greater than unity (Fig. 3). Implementation of the sliding mode control in this manner also provides input and output short-circuit protection.

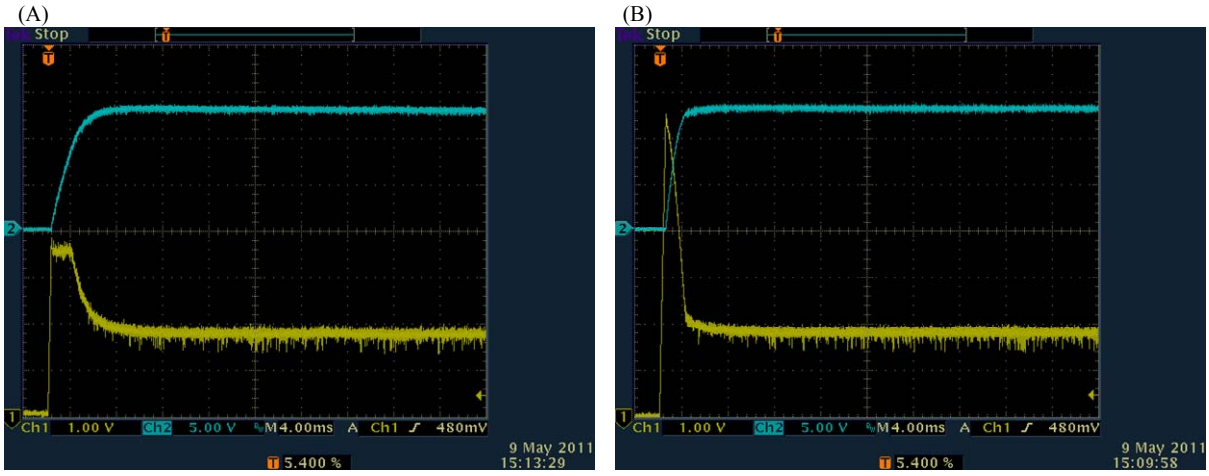

Fig. 3. System output voltage (top, 5 V / division) and inductor current (bottom, 1 A / division) responses at start up with (a) and without (b) current limit.

Until now it has been assumed that the inductor error signal is available for use by the controller. In reality the inductor current error component can be obtained by means of a high-pass filter which separates the high-frequency error deviations from the steady-state inductor current. This filter is described in further detail below.

Fig.4 shows an implementation of the above sliding-mode control law including inductor current limitation and high pass filter using standard logic components and three op-amp hysteresis comparators.

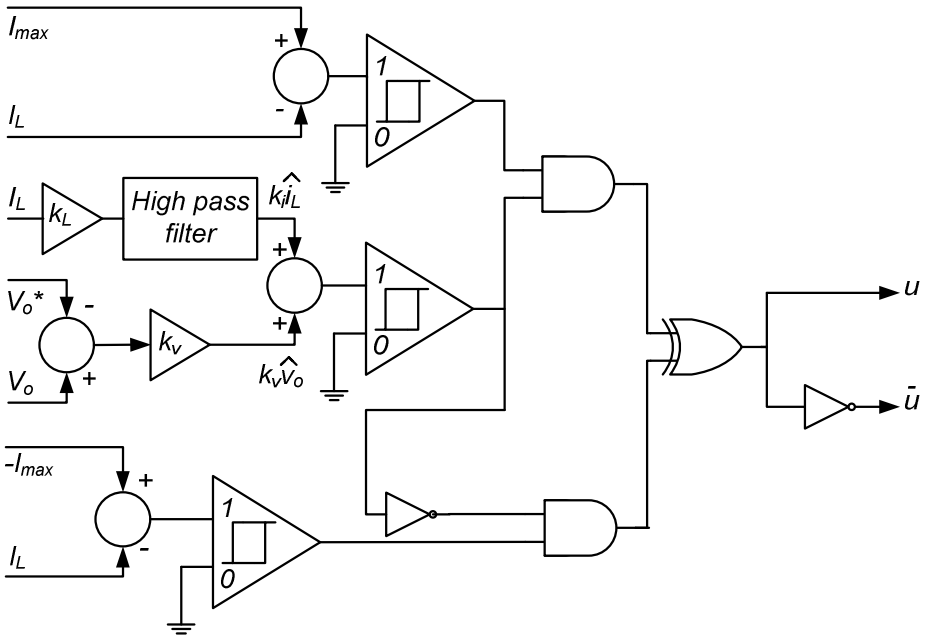

Fig. 4. Sliding mode control logic

System Stability and Dynamics

The equivalent control method described by Utkin [7] can be used to describe the average converter dynamics once in sliding mode control. By rearranging (2), the equivalent control u_{eq} can be written:

$$u_{eq} = 1 - \frac{\frac{v_o - v_b}{R} + C\frac{dv_o}{dt}}{i_L} \tag{13}$$

Substituting u_{eq} into (1) gives:

$$v_g i_L - L\frac{di_L}{dt}\cdot i_L = \frac{v_o - v_b}{R}(v_o + v_g) + C\frac{dv_o}{dt}(v_o + v_g) \tag{14}$$

Assuming that i_L can be approximated by its continuous average value and that $v_g >> L\frac{di_L}{dt}$ as used in [4], then (14) reduces to:

$$v_g i_L = \frac{v_o - v_b}{R}(v_o + v_g) + C\frac{dv_o}{dt}(v_o + v_g) \tag{15}$$

Substituting (3) in (14), an expression for the current error can be found in terms of the output voltage error and its derivative, by separating the steady state and error terms:

$$\hat{i}_L = \frac{\hat{v}_o}{Rv_g}(2V_o^* + \hat{v}_o + v_g - v_b) + \frac{C}{v_g}\frac{d\hat{v}_o}{dt}(V_0^* + \hat{v}_o + v_g) \tag{16}$$

$$I^* = \frac{(V_o^* - v_b)(V_o^* + v_g)}{Rv_g} \tag{17}$$

Substituting (16) into the sliding surface equation (4) yields a polynomial in terms of V_o and its derivative of the form:

$$\sigma = a\hat{v}_o + b\frac{d\hat{v}_o}{dt} = 0 \tag{18}$$

where:

$$a = k_v + \frac{k_i}{Rv_g}(2V_o^* + \hat{v}_o + v_g - v_b) \qquad b = k_i \frac{C}{v_g}(V_0^* + \hat{v}_o + v_g) \tag{19}$$

Let $V = \frac{\hat{v}_o^{\,2}}{2}$ be a Lyapunov candidate function, then:

$$\dot{V} = \hat{v}_o \frac{d\hat{v}_o}{dt} = -\frac{a}{b}\hat{v}_o^{\,2} \tag{20}$$

A sufficient condition for asymptotic stability on the sliding surface is that both *a* and *b* are of the same sign. The solution of (17) is then an exponential decay of the voltage error term towards zero such that the system converges to the steady state operating point (16). For this to be the case the following bounds on the magnitude of the voltage error term must be true:

$$k_v + \frac{k_i}{Rv_g}(2V_o^* + v_g - v_b) > -\hat{v}_o \tag{21}$$

$$(V_0^* + v_g) > -\hat{v}_o \tag{22}$$

The values of *a* and *b* from (19) determine the system response on the sliding line. The sliding mode equation (17) can be re-rewritten:

$$\hat{v}_o = -\frac{b}{a} \cdot \frac{d\hat{v}_o}{dt} \tag{23}$$

In the vicinity of the steady state operating point, the output error is small and $\hat{v}^2_o$ terms become very small and equation (15) can be approximated:

$$\hat{i}_L = c \cdot \hat{v}_o + d \cdot \frac{d\hat{v}_o}{dt} \tag{24}$$

where

$$c = \frac{1}{R \cdot v_g}(2V_o^* + \hat{v}_o + v_g - v_b) \tag{25}$$

and

$$d = \frac{C}{v_g}(V_0^* + v_g) \tag{26}$$

For small errors the system dynamics near the steady-state operating point are governed by the following differential equation:

$$\sigma' = k_v \cdot \hat{v}_o + k_i(\hat{v}_o \cdot c + \frac{d\hat{v}_o}{dt} \cdot d) = 0 \tag{27}$$

Until now the dynamics introduced by the incorporation of the high-pass filter have not been considered. This study now considers adding a first-order filter which affects the system dynamics as shown by the following Laplace-domain equation:

$$\sigma''(s) = k_v \cdot \hat{v}_o(s) + \frac{s}{(s+\omega)} \cdot k_i \cdot i_L(s) = 0 \tag{28}$$

In the vicinity of the steady state operating point the dynamics of motion on the sliding line (27) incorporating high-pass filter current measurement can be written in terms of the output voltage error in the Laplace domain as follows:

$$\sigma''(s) = \hat{v}_o(s)\left[k_v + k_i \frac{s}{(s+\omega)}(c+ds)\right] = 0 \tag{29}$$

$$\sigma''(s) = \frac{k_v \hat{v}_o(s)}{(\frac{\omega}{s}+1)}\left[(\frac{\omega}{s}+1) + \frac{k_i}{k_v}c + \frac{k_i}{k_v}ds\right] = 0 \tag{30}$$

The system response is second order, due to the incorporation of the filter dynamics. If the operating point of interest and load are known, then a choice of filter corner frequency which allows the system response to resemble a first order response is:

$$\omega = \frac{c}{d} \tag{31}$$

If ω is set as (31) and substituted into (30), the following simplification by factorisation is possible:

$$\sigma''(s) = \frac{k_v \hat{v}_o(s)}{\left(\frac{\omega}{s}+1\right)}\left[\left(\frac{\omega}{s}+1\right)\left(1+\frac{k_i}{k_v}ds\right)\right] = 0 \tag{32}$$

$$\sigma''(s) = \hat{v}_o(s)[k_v + k_i ds] = 0 \tag{33}$$

The response is a first order exponential decay of the error term with time constant:

$$\tau' = -\frac{k_i}{k_v}d \tag{34}$$

Effect of hysteresis band on converter switching frequency

In the theoretical ideal case the converter would switch at infinite frequency. A more practical implementation of the sliding surface incorporates control of the frequency of oscillation. There are various ways of achieving this but the method employed here is to incorporate a hysteresis band. If the hysteresis width is *h*, the switching control law (6) is then implemented as:

$$u = \begin{cases} 1, & if \quad \sigma < -h \\ 0, & if \quad \sigma > h \end{cases} \tag{35}$$

The addition of the hysteresis band causes the system motion on the sliding surface to deviate from the ideal case presented above. The assumption that the system motion approximates closely the ideal case remains valid if the hysteresis band is small so this then becomes a design requirement. The switching period is the sum of inductor-current rise, *T1,* and inductor-current fall, *T2.* It has been shown [7] that the switching frequency can be calculated by substituting (7) and (8) into (24) and (25) to give:

$$T_1 = \frac{2h}{\dot{[\sigma]}_{u=1}} \qquad (36) \qquad T_2 = \frac{-2h}{\dot{[\sigma]}_{u=0}} \qquad (37)$$

The minimum switching frequency for a given set of operating conditions can be found using (36) and (37) and this places a maximum value for the upper bound of the inductor current error measurement filter corner frequency.

Simulated and Measured Results

To investigate the operation of the DC-to-DC converter, a prototype was developed initially switching at a low frequency of about 5 kHz. The converter operation is then optimised by reducing the hysteresis band to increase the switching frequency and reduce current ripple. Voltage source V_b in Fig.1 is a lead-acid battery with open-circuit voltage of 13V DC and the resistor R is set to 1 Ω for the purpose of this demonstration. The key parameters values and components are given in Appendix 1, Table 1. The same converter is then modelled in Matlab/Simulink [8] using elements from the Simpower Systems Toolbox, then an average model of the converter is created by implementing the dynamic equations (28) and (27). The results are shown in Fig. 5 and both the full order switching simulation and measured results can be seen to verify the averaged model. Using the relevant values from Appendix 1, Table 1. and equation (34), the predicted time constant of the response is 5.9 x 10^{-4}s which is in good agreement with the time constant of the measured response (Fig. 5a), the switching model (Fig. 5b) and average response (Fig. 5c). An improvement to the average model could be to model the slew rate of the inductor current, and this is the subject of future work.

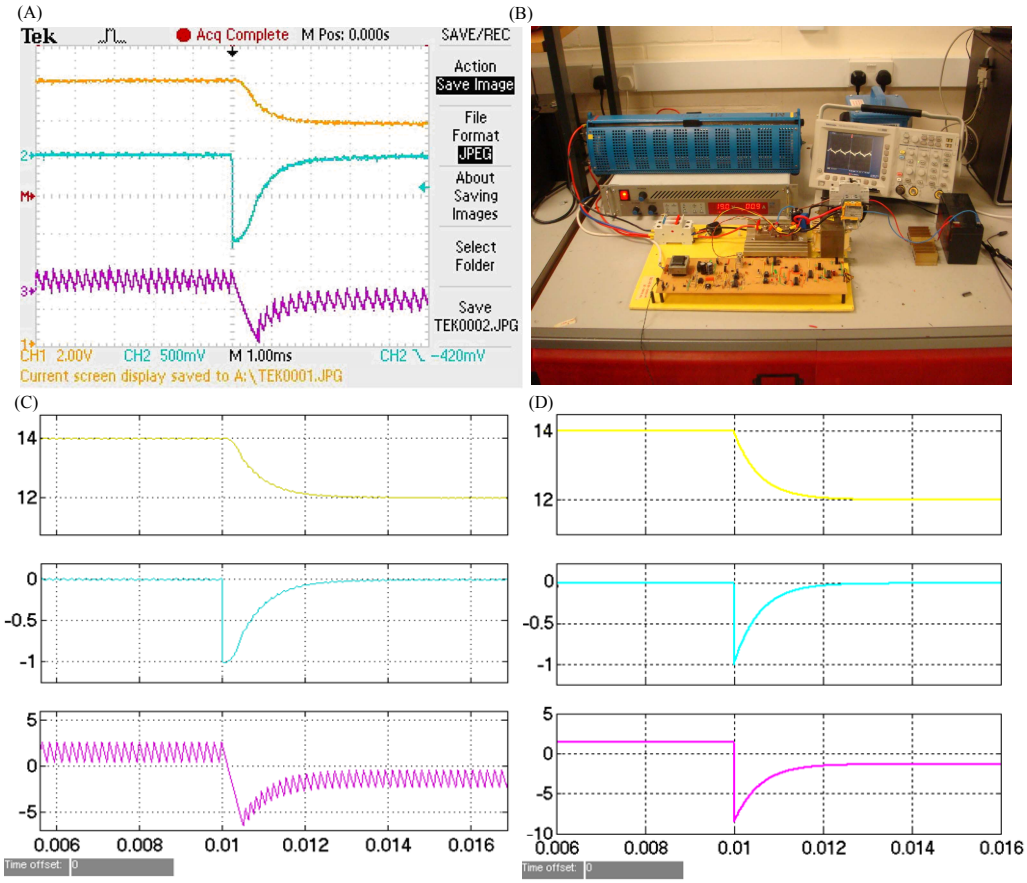

Fig 5. a) Measured response. b) Experimental set up c) Simulated switching response d) Average simulated response. (Yellow trace: Output voltage 2v / div. Cyan: Voltage error signal: 0.5V/div. Magenta: Inductor current 5A/div.)

Having verified the basic operation of the converter, the hysteresis band is reduced to reduce current ripple and further tests are carried out with the results shown in Fig. 6. The response of the converter to a 2 V command step is measured with different current error filter cut off frequencies (optimal, higher and lower than optimal). If the filter cut-off frequency is chosen using (31), the response shown in Fig. 6 (a) resembles that of a first-order system, whereas with the cut-off frequency set higher (see Fig 6b) or lower (see Fig. 6c), the response resembles that of a higher order system. With the cut-off frequency set higher than the optimal, the system response tends to converge in an oscillatory manner and with the cut frequency set too low the response is overdamped and has a slow rise time.

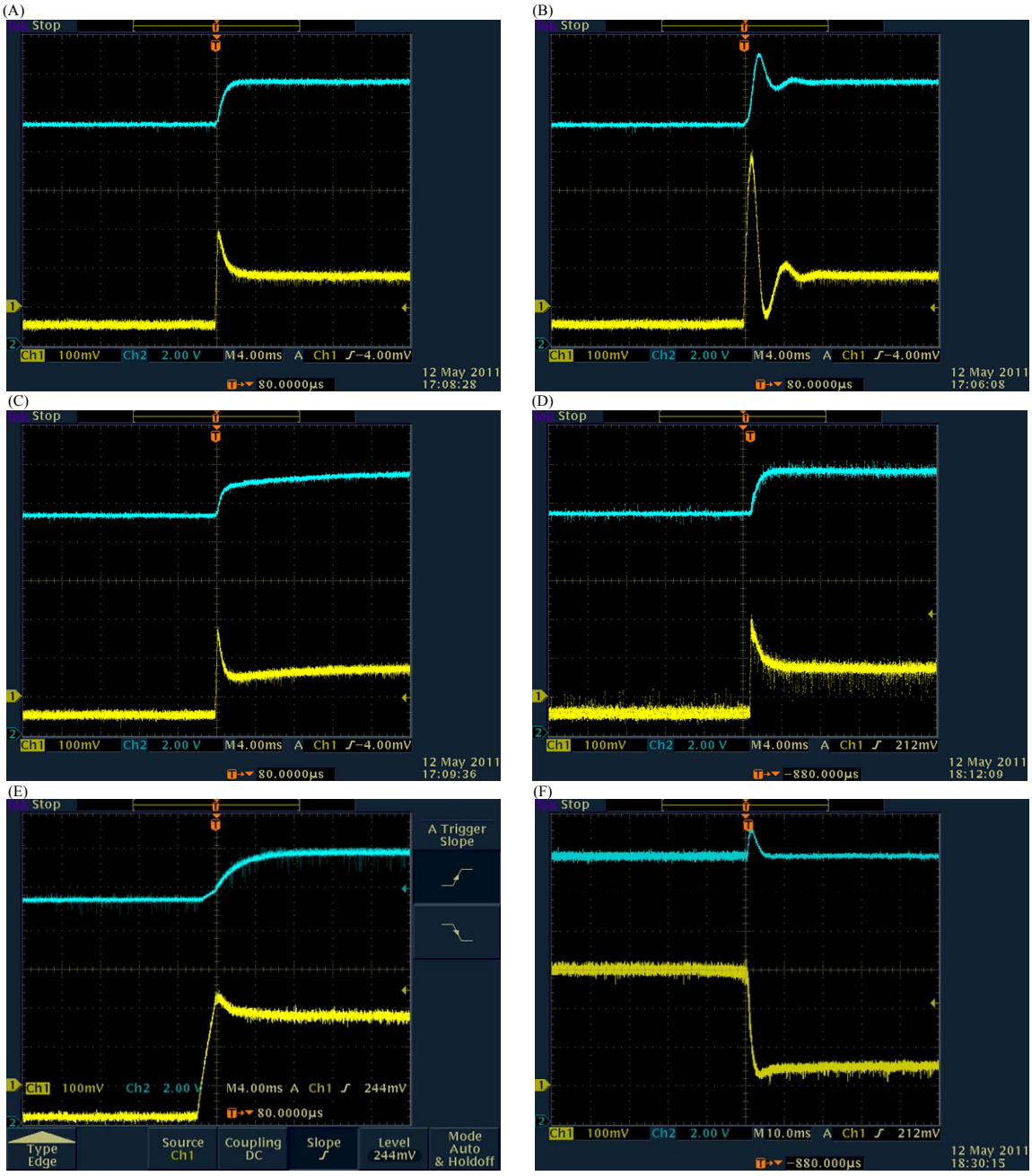

Fig. 6. Step response 12 – 14 V: a) Optimal filter cut off frequency = $\omega_{opt.}$ b) Filter cut off frequency = $2\ \omega_{opt.}$ c) Filter cut off frequency = $\omega_{opt}\ /\ 2$. d) Input voltage Vg = 100 Vdc. e) Input voltage Vg = 5 Vdc f) Step load resistance change 0.3Ω to 1Ω V_o = 14 Vdc.
(Yellow trace = Output Voltage 2 V / division. Cyan trace = Inductor current 2 A / division).

Next the filter cut off frequency is reset to the optimal value and the converter is tested at two different input voltage levels (Fig. 6f and 6g). At 100 V input voltage the form of the response can be seen to be consistent with the response at the nominal input voltage of 30 V. At 5 V input voltage the delay in

current error tracking due to the slew rate of the inductor starts to become significant and indicates that for operation at this voltage level the inductance should ideally be decreased. Finally the converter response to a step load change from 0.3Ω to 1Ω shows that the system tracks from one region of operation to the other successfully.

Conclusions

A novel implementation of a sliding mode voltage controller with bidirectional current-control capability and input and output current limiting has been developed. A simple and cost effective hardware realisation using standard logic gates and op-amps has been presented. A technique for current-error filter cut-off frequency selection has been given which allows the resulting hardware implementation to closely approximate to the theoretical case of a reduced order response once the system is in sliding mode. The system response has been shown experimentally to be relatively robust and have a similar form over a wide range of input voltage conditions.

Applications include renewable energy storage systems, uninterruptable power supply systems, electric vehicle energy storage systems, battery charge and discharge circuits or applications in which one variable voltage source is interfaced to another. In supercapacitor applications where the supercapacitor voltage can be higher or lower than the required output voltage, this converter design can be used to successfully charge and discharge the supercapacitor and utilise the full energy stored due to its wide input voltage range tolerance. This is the subject of current and on-going future work.

Future work also includes the development of an inductor-current slew rate model and application of this control theory to consider a galvanically isolated version of the converter in which the inductor is replaced by an isolating transformer.

References

[1] Wester, G.W. and Middlebrook, R.D., *Low-Frequency Characterization of Switched dc-dc Converters.* Aerospace and Electronic Systems, IEEE Transactions on, 1973. **9**(3): pp. 376-385.

[2] Alvarez-Ramirez, J., Cervantes, I., Espinosa-Perez, G., Maya, P. and Morales, A., *A stable design of PI control for DC-DC converters with an RHS zero.* Circuits and Systems I: Fundamental Theory and Applications, IEEE Transactions on, 2001. **48**(1): pp. 103-106.

[3] Ridley, R.B., *A new, continuous-time model for current-mode control [power convertors].* Power Electronics, IEEE Transactions on, 1991. **6**(2): pp. 271-280.

[4] Venkataramanan, R., Sabanovic, A. and Cuk, S., *Sliding-mode control of power converters.* Indian Institute of Science, Journal 1989. **69**(0019-4964): pp. 193-211.

[5] Tsai, J.-F. and Chen, Y.P., *Sliding mode control and stability analysis of buck DC-DC converter.* International Journal of Electronics, 2007. **94**(3): pp. 209 - 222.

[6] Sabanovic, A., Fridman, L., and Spurgeon, S., *Variable Structure Systems: From Principles to Implementation*. 2004, Stevenage: Institution of Engineering and Technology (IET).

[7] Utkin, V., *Sliding modes in control and optimization* 1992, Berlin: Springer-Verlag.

[8] *MATLAB v7.10*. 2010, The MathWorks Inc. Natick, MA.

Appendix 1. Table I. Parameter values and key component list of prototype design.

Parameter	Value
R	1Ω
C1= C2	2000μF
L	1.8mH
Vg	30Vdc
Ki	0.1
Kv	0.5
Hysteresis width, h	100mV

Component	Part number
Comparator	LM339N
IGBT module	FUJI 2MBI75S-120-50
Gate drive	IR21844
Logic gates: NOR	HEF4001BP
Logic gates: XOR	HEF4070BP
Current transducer	LEM LA100-P/SP13
Voltage transducer	LEM LV 25-P 16195